Neurobiology of Disease 130 (2019) 104497

Contents lists available at ScienceDirect

Neurobiology of Disease

journal homepage: www.elsevier.com/locate/ynbdi

β-catenin aggregation in models of ALS motor neurons: GSK3β inhibition effect and neuronal differentiation

Cristina Pinto[a], Danilo B. Medinas[b,c,d], Francisco Fuentes-Villalobos[e], Jaime Maripillán[f], Ariel F. Castro[e], Agustín D. Martínez[f], Nelson Osses[g], Claudio Hetz[b,c,d,h,i], Juan P. Henríquez[a,*]

[a] Neuromuscular Studies Laboratory (NeSt Lab), Center for Advanced Microscopy, Faculty of Biological Sciences, Department of Cell Biology, Universidad de Concepción, Concepción, Chile
[b] Biomedical Neuroscience Institute (BNI), Faculty of Medicine, University of Chile, Santiago, Chile
[c] Center for Geroscience, Brain Health and Metabolism (GERO), Santiago, Chile
[d] Program of Cellular and Molecular Biology, Institute of Biomedical Sciences, University of Chile, Santiago, Chile
[e] Departamento de Bioquímica y Biología Molecular, Facultad de Ciencias Biológicas, Universidad de Concepción, Concepción, Chile
[f] Centro Interdisciplinario de Neurociencia de Valparaíso, Instituto de Neurociencia, Facultad de Ciencias, Universidad de Valparaíso, Valparaíso, Chile
[g] Institute of Chemistry, Faculty of Sciences, Pontificia Universidad Católica de Valparaíso, Valparaiso, Chile
[h] The Buck Institute for Research in Aging, Novato, CA 94945, USA
[i] Department of Immunology and Infectious Diseases, Harvard School of Public Health, Boston, MA 02115, USA

ARTICLE INFO

Keywords:
β-Catenin
Accumulation
ALS
Motor neuron
GSK3β inhibition
Differentiation

ABSTRACT

Amyotrophic lateral sclerosis (ALS) is a neurodegenerative disease characterized by motor neuron death. A 20% of familial ALS cases are associated with mutations in the gene coding for superoxide dismutase 1 (SOD1). The accumulation of abnormal aggregates of different proteins is a common feature in motor neurons of patients and transgenic ALS mice models, which are thought to contribute to disease pathogenesis. Developmental morphogens, such as the Wnt family, regulate numerous features of neuronal physiology in the adult brain and have been implicated in neurodegeneration. β-catenin is a central mediator of both, Wnt signaling activity and cell-cell interactions. We previously reported that the expression of mutant SOD1 in the NSC34 motor neuron cell line decreases basal Wnt pathway activity, which correlates with cytosolic β-catenin accumulation and impaired neuronal differentiation. In this work, we aimed a deeper characterization of β-catenin distribution in models of ALS motor neurons. We observed extensive accumulation of β-catenin supramolecular structures in motor neuron somas of pre-symptomatic mutant SOD1 mice. In cell-cell appositional zones of NSC34 cells expressing mutant SOD1, β-catenin displays a reduced co-distribution with E-cadherin accompanied by an increased association with the gap junction protein Connexin-43; these findings correlate with impaired intercellular adhesion and exacerbated cell coupling. Remarkably, pharmacological inhibition of the glycogen synthase kinase-3β (GSK3β) in both NSC34 cell lines reverted both, β-catenin aggregation and the adverse effects of mutant SOD1 expression on neuronal differentiation. Our findings suggest that early defects in β-catenin distribution could be an underlying factor affecting the onset of neurodegeneration in familial ALS.

1. Introduction

Amyotrophic lateral sclerosis (ALS) is a neurodegenerative disease characterized by the selective death of motor neurons in the spinal cord, brainstem and motor cortex. This progressive disease causes atrophy of limb, axial and respiratory muscles (Kiernan et al., 2011). Most ALS cases are considered sporadic (sALS), while 10% are familial (fALS), involving mutations in superoxide dismutase 1 (SOD1), transactive response DNA binding protein 43 (TARDBP or TDP-43), fused in sarcoma/translocated in sarcoma (FUS/TLS), and the hexanucleotide repeat expansions in C9ORF72 as the most common alterations (Al-Chalabi and Hardiman, 2013; Turner et al., 2013). > 150 mutations in SOD1 have been linked to ALS with varying degree of aggressiveness and aggregation propensity, which explains around 20% of fALS cases (Valentine et al., 2005). Importantly, several studies have reported the presence of abnormal $SOD1^{WT}$ species in post-mortem sALS tissue highlighting the relevance of the protein in disease pathogenesis (Bosco et al., 2010; Ciechanover and Kwon, 2015; Forsberg et al., 2010;

* Corresponding author at: Department of Cell Biology, Faculty of Biological Sciences, Universidad de Concepcion, Casilla 160-C, Concepcion, Chile.
E-mail address: jhenriquez@udec.cl (J.P. Henríquez).

https://doi.org/10.1016/j.nbd.2019.104497
Received 13 January 2019; Received in revised form 26 May 2019; Accepted 5 June 2019
Available online 07 June 2019
0969-9961/

Medinas et al., 2018). Mice overexpressing mutant SOD1 are the most widely used model of ALS as they develop consistent motor neuron degeneration and clinical progression resembling the human disease (Gurney et al., 1994). Despite many efforts, the mechanisms by which SOD1 mutations lead to motor neuron degeneration are not yet fully understood.

Insoluble protein aggregates and inclusion bodies are hallmarks of several neurodegenerative diseases such as ALS, including Alzheimer's disease (AD), Parkinson's disease (PD), Huntington's disease (HD) and spino-cerebellar ataxia (Soto, 2003). Protein aggregates may have different nature according to the mechanism involved in their assembly (Bendotti et al., 2012). Indeed, deficient ubiquitin-proteasome system (UPS), impaired autophagy, and abnormal RNA-binding proteins assembling into stress granules have been implicated in the formation of protein aggregates in ALS (Taylor et al., 2016). Although protein aggregation has been described near the onset of ALS symptoms, growing evidence demonstrates that several cellular alterations take place at pre-symptomatic stages. These include mitochondrial dysfunction, Golgi fragmentation, endoplasmic reticulum stress, increased neuronal excitability, and neuromuscular junction detachment (Amendola et al., 2004; Dobrowolny et al., 2017; Hetz and Saxena, 2017; Kuo et al., 2004; Moloney et al., 2014; Pambo-Pambo et al., 2009; van Zundert et al., 2008). Thus, defining early molecular defects in ALS motor neurons is crucial to reveal the primary mechanisms of the disease and to identify novel targets for therapeutic intervention.

Neuronal physiology is tightly controlled by morphogens of early development, such as the Wnt family (Inestrosa and Arenas, 2010). The canonical Wnt pathway is activated by the binding of a Wnt ligand to a cognate Frizzled receptor (Fzd) and to LRP5/6 co-receptors, resulting in cytosolic glycogen synthase kinase-3β (GSK3β) inhibition and induction of a cytoplasmic accumulation of β-catenin, whose nuclear translocation regulates the expression of target genes. Gene expression profile analyses of spinal cord tissue derived from mutant SOD1 mice have revealed a global increase in the expression of Wnt ligands, receptors, and inhibitors at symptomatic stages of the disease (Al-Chalabi and Hardiman, 2013; González-Fernández et al., 2019; Li et al., 2013); however, the possible consequences of Wnt pathway alterations in ALS motor neurons have been less explored. We previously reported that the expression of mutant SOD1 in NSC34 motor neuron-like cells results in impaired basal Wnt-dependent transcriptional activity, a feature that correlated with β-catenin distribution in macromolecular structures, particularly in undifferentiated cells (Pinto et al., 2013).

Here, we aimed at a deeper characterization of β-catenin distribution in ALS models. Our findings indicate that motor neuron somas of pre-symptomatic and symptomatic stages of ALS mice display supramolecular β-catenin structures. Although co-localization and biochemical experiments showed that β-catenin does not form classical protein aggregates, its distribution in the cell periphery of clustered cells correlated with decreased cell-cell adhesion and increased cell coupling. Remarkably, GSK3β inhibition reverted β-catenin accumulation and rescued normal neuronal differentiation. Our findings suggest that early alterations of β-catenin distribution may contribute to ALS pathogenesis.

2. Materials and methods

2.1. Animals and spinal cord sections

As an *in vivo* model of ALS, transgenic mice expressing human SOD1^{G93A} were used. Mice expressing the WT form of human SOD1 were used as controls. The animal care and all animal experiments were performed according to procedures approved by the "Guide for the Care and Use of Laboratory Animals" (Commission on Life Sciences, National Research Council. National Academy Press 1996) and approved by the Bioethical Committee of the Faculty of Medicine, University of Chile. Spinal cord tissue was dissected, fixed in 4% paraformaldehyde in PBS and incubated in a sucrose gradient (from 7.5 to 30% in PBS). Samples were mounted in OCT (Sakura Finetek, Torrance, CA, USA) and 30 µm sections were obtained from the lumbar L5 region.

2.2. Cell culture and treatments

Neuroblastoma x spinal cord NSC34 cells (Cashman et al., 1992), as well as clones stably expressing human wild-type SOD1 (NSC34-hSOD1^{WT} cells) or mutant SOD1 (NSC34-hSOD1^{G93A} cells) (Gomes et al., 2008) were grown in Dulbecco's modified Eagle's medium (DMEM) (HyClone, South Logan, UT, USA) supplemented with 15% fetal bovine serum (FBS), 1% penicillin/streptomycin solution at 37 °C in a 5% CO_2 atmosphere. Stable clones were supplemented with 0.4 mg/ml G418. Cells were grown on plastic or glass surfaces previously coated with 0.01% poli-L-lysine (Sigma-Aldrich, MO, USA) for 24 h at 37 °C, and 0.5% gelatin (Sigma-Aldrich) for 30 min at 37 °C. Cells were induced to differentiate in Neurobasal medium (Invitrogen, MA, USA) without FBS for 24 h. In disassembly experiments, cells were washed twice with saline phosphate buffer (PBS), pH 7.4, and incubated in fresh growth medium containing 40 mM lithium chloride or 10 µM andrographolide (ANDRO) (both from Sigma-Aldrich) for 6 h at 37 °C in a 5% CO_2 atmosphere. In cell differentiation assays, cells were incubated with 2 µM ANDRO or 100 µM lithium chloride for 24 h (De Ferrari et al., 2003; Tapia-Rojas et al., 2015). Stress granule formation was induced by incubating cells with DMEM supplemented with 0.5 mM $NaAsO_2$ (Sigma-Aldrich) for 45 min at 37 °C (Tourrière et al., 2003). The proteasome inhibitor MG132 was diluted in growth medium at a final concentration of 10 µM and incubated for 6 h at 37 °C (Onesto et al., 2011).

2.3. Transient transfection

NSC34 cells were seeded onto glass coverslips in 24 well plates, grown for 24 h, and transfected with a lipofectamine-PLUS mixture (Invitrogen) in OptiMEM medium (Invitrogen) according to the instructions of the manufacturer. We used the pF141 pAcGFP1 SOD1^{WT} and the pF145 pAcGFP1 SOD1^{G93A} plasmids (Addgene, plasmids #26402 and #26406) (Stevens et al., 2010). The DNA/lipofectamine/PLUS ratio in the mixture was 0.4 µg/1.2 µl/0.8 µl with 0.4 µg of total plasmid DNA per well. Cells were incubated with the DNA mixture and lipofectamine-PLUS in serum-free medium for 4 h before being switched to the growth medium. When indicated, cells were switched to differentiate for the indicated times.

2.4. Western blot analysis

Cells were lysed in PBS (cytosolic extract), or in Tris-HCl 50 mM, NaCl 100 mM, Triton X-100 0.5% v/v (total extract), pH 7.4, supplemented with a protease inhibitor cocktail (Sigma-Aldrich). For immunoblotting, 10 µg of total proteins were loaded in each lane, fractionated by SDS-PAGE, transferred onto nitrocellulose membranes, and probed against rabbit anti β-catenin (1:1000) (Santa Cruz Biotechnology, CA, USA) and mouse anti α-tubulin (1:5000) (Sigma-Aldrich) antibodies. Peroxidase-conjugated secondary antibodies (1:2000) (Jackson Immunoresearch, PA, USA) were incubated for 2 h at room temperature. Reactions were developed with enhanced chemiluminiscence according to the ECL Western blotting analysis system (Perkin Elmer, MA, USA).

2.5. Filter-trap analysis

Protein extracts were prepared in TEN buffer (Tris-HCl 10 mM, EDTA 1 mM, NaCl 100 mM, pH 8.0) containing Nonidet P-40 0.5% (v/v) and protease inhibitor cocktail (Promega, WI, USA) by ultra-sonication at 30% power during 15 s (QSonica, NY, USA). Protein concentration was measured using the BCA assay according to

manufacturer's instructions (Pierce, MA, USA). For filter-trap, the samples were diluted in PBS, pH 7.4, containing SDS 1% (w/v) or Nonidet P-40 1% (v/v) to a final concentration of 0.5 μg/ml and passed through a cellulose acetate membrane with 0.22 μm pore (Whatman, Buckinghamshire, UK) under vacuum using a dot-blot apparatus (Bio-Rad, CA, USA) (Medinas et al., 2018). After filtration, the membranes were washed in PBS, pH 7.4, containing SDS 1% (w/v) for 15 min, followed by three washes in PBS, pH 7.4, containing Tween 0.1% (v/v), blocked with skim milk 5% (w/v) in PBS, pH 7.4, and incubated with mouse anti β-catenin (1:1000) (Millipore, Darmstadt, Germany) overnight at 4 °C. Detection was performed with peroxidase-conjugated secondary antibodies (1:2000) (Invitrogen) and ECL kit (Perkin Elmer, MA, USA) using the ChemiDoc imaging system (Bio-Rad, CA, USA).

2.6. Detergent-insoluble protein aggregates

Post-nuclear protein extracts were prepared by cell lysis in TEN buffer containing Nonidet P-40 0.5% (v/v) and protease inhibitor cocktail (Promega, WI, USA) during 30 min on ice followed by low-speed centrifugation (800 ×*g*, 10 min, 4 °C) to remove nucleus and cell debris (P1). The supernatant was collected and centrifuged at high-speed (20,000 ×g, 45 min, 4 °C) to yield a pellet (P2) containing Nonidet P-40 insoluble protein aggregates. The P2 pellet was solubilized in TEN buffer containing SDS 1% (w/v) and analyzed by Western-blot, as described (Medinas et al., 2018).

2.7. Cell-cell interaction experiments

NSC34-hSOD1^{WT} or NSC34-hSOD1^{G93A} cells were seeded onto 35 mm plastic dishes and grown to reach confluency. In separate dishes, both NSC34-hSOD1 cell lines were stained with Calcein AM-488 (Waltham, MA USA) for 20 min at 37 °C. After trypsinization, 2×10^5 cells were seeded on top of the monolayers of their same cell line and incubated for 30 min. After removing non-adhered cells by washing, adhered cells were fixed in paraformaldehyde 4%, 20 min at 4 °C, and mounted in Faramount aqueous mounting medium (DAKO, CA, USA). Cell-cell adhesion index was determined by counting the number of Calcein positive cells attached to the monolayer. Intercellular coupling was examined after microinjection of the gap junction tracers Lucifer Yellow (LY, MW: 457, net charge: −2) and neurobiotin (MW: 345, net charge: +1), as previously described (Martinez et al., 2002). Tracers were injected in one cell inside a group of at least 6 cells. The transfer of LY was detected after 2 min by epifluorescence. Cells were fixed with paraformaldehyde 4%, 20 min at 4 °C and neurobiotin was traced with Cy3-conjugated streptavidin (Jackson Immunoresearch West Grove, PA, USA) after permeabilization with 0.25% Triton-X100 in PBS. The dye-coupling index was calculated as the number of coupled or dye-filled cell groups divided by the total number of dye-injected cells per conditions. Over 60 injected cells per condition of three independent experiments were analyzed.

2.8. Inmunohistochemistry, immunofluorescence microscopy and image analysis

For immunohistochemistry, floating spinal cord cryosections were repeatedly washed with PBS containing 0.1% Tween-20, incubated with 0.15 mM glycine, pH 7.4, for 15 min at room temperature, and blocked with 1% BSA diluted in Tris phosphate buffer. NSC34-hSOD1 cells were grown on 18 × 18 mm glass coverslips, fixed in 4% paraformaldehyde for 20 min at 4 °C, followed by 100% methanol at −20 °C for 5 min, and permeabilized with 0.05% Triton X-100 in Tris-phosphate buffer. Primary antibodies were: rabbit anti β-catenin 1:1000 (Millipore), mouse anti-neurofilament 1:50 (2H3, Developmental Studies Hybridoma Bank), goat anti-ChAT 1:250 (Merck, Darmstadt, Germany), rabbit anti-Connexin-43 1:500 (Sigma-Aldrich), mouse anti-E-cadherin 1:100 (Biosciences, CA, USA), mouse anti β-catenin 1:200, mouse anti-γ-tubulin 1:100, goat anti-MAP1B 1:450, rabbit anti-Ubiquitin 1:100, goat anti-TIA1 1:300 (Santa Cruz Biotechnology), and rabbit anti-eIF3h 1:300 (Cell Signaling Technology, MA, USA). Primary antibodies were incubated in 1% BSA diluted in Tris phosphate for 16 h at 4 °C. Corresponding Alexa-488, Alexa-546 (Invitrogen) and Cy5 (Jackson Immunoresearch) conjugated secondary immunoglobulins were incubated for 2 h at room temperature. Nuclei were counterstained with 30 μM DAPI (Molecular Probes, MA, USA) along with the secondary antibodies. Samples were mounted in DAKO aqueous medium. Images were captured in a laser confocal LSM780 Zeiss microscope at the Center for Advanced Microscopy (CMA Bio-Bio) facility at Universidad de Concepción (Concepción, Chile). In the *in vivo* model, β-catenin structures were defined as those having an area larger than 0.2 μm^2 and were quantified in ChAT positive neurons. In the *in vitro* model, β-catenin structures were defined as those having an area larger than 0.2 μm^2 and were quantified in cell groups containing at least 6 cells. In each condition, β-catenin structures were selected using the threshold function of ImageJ to quantify their number and size. The number of differentiated cells and the length of their neurites were determined in cells having at least one neurite with a minimum size equal to the cell soma diameter (Benavente et al., 2012; Pinto et al., 2013). Stress granules were defined as those exhibiting eIF3h and TIA1 co-localization, and were quantified as the percentage of cells bearing them and as the number of stress granules per cell. In cell-cell adhesion experiments, the number of Calcein AM-488 positive cells adhered to a 10,000 μm^2 region of interest (ROI) of the corresponding cell line monolayer was quantified. Co-localization analyses were performed in double staining (β-catenin/E-cadherin and β-catenin/Connexin-43) for three independent cultures per condition. In each *z* plane of consecutive confocal image series, circular ROIs were analyzed in appositional (cell-cell contacts) and non-appositional (nucleus periphery) areas of two contacting cells to measure Mander's Coefficient using the Image J software. To obtain E-cadherin or Connexin-43 over β-catenin Mander's overlapping values, a total of 20 to 60 ROIs of appositional and non-appositional areas were quantified. Merge images were processed with the Imaris software to filter co-localization regions in each *z* plane of consecutive confocal image series.

2.9. Statistical analyses

Experiments with NSC34-hSOD1 cells were performed at least three times by triplicate. In each condition, 10–15 fields per coverslip were quantified. Plots correspond to the mean ± SEM. One-way ANOVA or two-way ANOVA was used for comparison among three or more groups followed by Bonferroni's *post hoc* analysis for multiple comparisons between different groups. The number and size of β-catenin structures, the percentage of cell groups having β-catenin structures, cell adhesion, cell coupling, and the ratio of β-catenin/α-tubulin bands in Western blot experiments, were compared using paired *t*-test. $p < 0.05$ was considered to indicate statistical significance.

3. Results

3.1. β-catenin distributes in supramolecular structures in cells expressing SOD1^{G93A} in cellular and animal models of ALS

To further characterize the accumulation of β-catenin structures in an ALS context, we first analyzed spinal cord samples from mice expressing the G93A mutation of human SOD1 (hSOD1^{G93A}) (Gurney et al., 1994). Immunostaining was performed in spinal cord sections obtained at P76 (pre-symptomatic) and P130 (symptomatic) stages from hSOD1^{G93A} and control mice, which express the wild-type (WT) form of hSOD1 (Fig. 1A). We immunodetected ChAT to identify motor neurons in the ventral horn of the spinal cord (Houser et al., 1983). β-catenin staining showed a nuclear and homogenous cytosolic distribution in spinal cord sections from control mice at both ages. In turn,

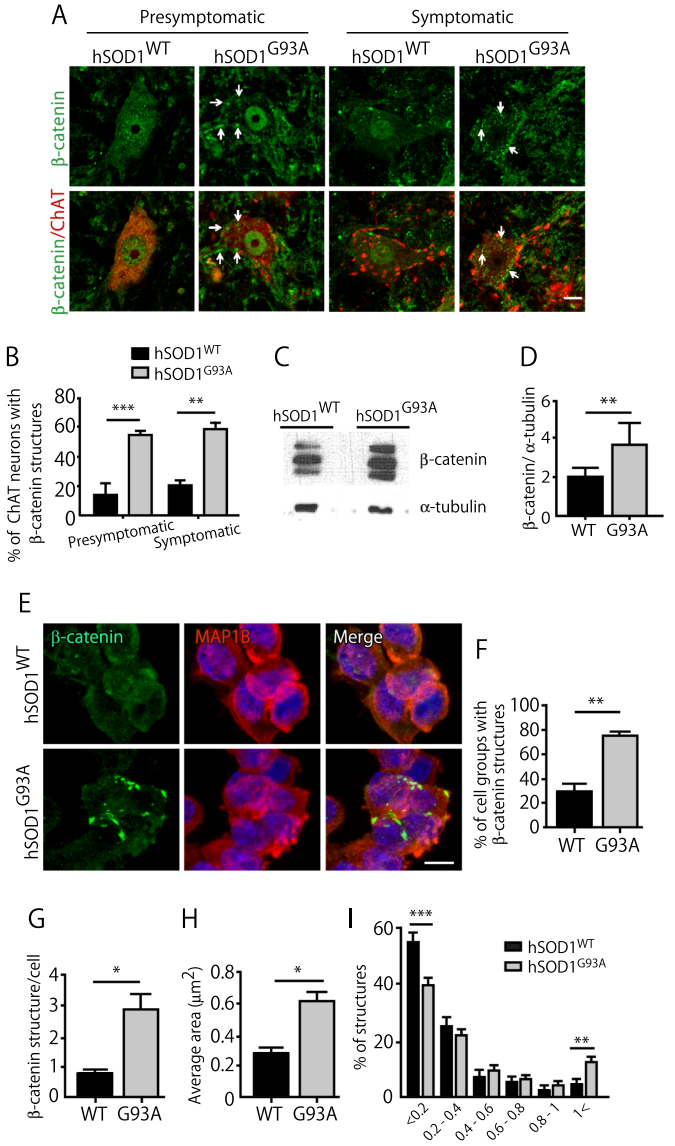

Fig. 1. β-catenin organizes in supramolecular structures in motor neurons of hSOD1^{G93A} mutant mice and ALS-like NSC34-hSOD1^{G93A} cells.
(A) Sections of control and hSOD1^{G93A} mutant mice at pre-symptomatic (P76) and symptomatic (P130) stages were stained with antibodies to detect β-catenin and ChAT. (B) Quantification of the percentage of motor neurons that display β-catenin structures. Data are expressed as the mean ± SEM of three independent experiments (**$p < 0.01$; ***$p < 0.001$). (C) Cytosolic protein fractions from NSC34-hSOD1^{G93A} and control NSC34-hSOD1^{WT} cells were analyzed by Western blot using a specific antibody to detect β-catenin. The levels of α-tubulin were used as loading control. (D) Quantification of the relative levels of β-catenin was performed by band intensity densitometry and expressed as a ratio regarding α-tubulin band intensity. Data are expressed as the mean ± SEM of three independent experiments (**p < 0.01). (E) NSC34hSOD1 cells were fixed and subsequently subjected to immunocytochemistry using anti β-catenin and anti-MAP1B antibodies. Nuclei were counterstained with DAPI. Quantifications show (F) the percentage of β-catenin positive cell groups, (G) the number of β-catenin aggregate-like structures per cell, (H) their average area, and (I) their size distribution. Data are the mean ± SEM of three independent experiments (*$p < 0.05$, **p < 0.01, ***p < 0.001, *t*-test). Scale Bars = 10 μm (A,E).

motor neurons from P76 hSOD1^{G93A} mice showed a clear cytosolic redistribution of β-catenin to the periphery of motor neuron somas (arrows in Fig. 1A). At P130, cytosolic β-catenin shows a punctate pattern in motor neurons from hSOD1^{G93A} mice, a feature that correlated with decreased nuclear distribution. Quantification shows a marked increase of β-catenin structures in ALS motor neurons (Fig. 1B). We also observed that β-catenin detection increased in surrounding cells (Fig. 1A). Thus, β-catenin distribution is altered in motor neurons of a mouse model of ALS.

In order to explore on β-catenin distribution under mutant SOD1^{G93A} expression, we performed detailed investigation in the NSC34 motor neuron-like cell line. As a first hint to characterize β-catenin accumulation in NSC34-hSOD1^{G93A} cells, total cytosolic protein fractions from ALS-like NSC34-hSOD1^{G93A} and control NSC34-hSOD1^{WT} cells were subjected to Western blot analyses to detect the cytosolic levels of β-catenin, whereas α-tubulin detection was used as loading control (Fig. 1C). Quantification of the band intensity of β-catenin/α-tubulin ratio shows a significant increase of β-catenin in NSC34-hSO1^{G93A} cells, compared to control cells (Fig. 1D). Immunocytochemistry experiments confirmed previous findings showing that β-catenin structures were abundant in undifferentiated NSC34-hSOD1^{G93A} cells (Fig. 1E). Quantification reveals a striking increase in the abundance (Fig. 1F), number (Fig. 1G), as well as of the average area of β-catenin structures in NSC34-hSOD1^{G93A} cells, compared to controls (Fig. 1H). Histogram analyses revealed that NSC34-hSOD1^{G93A} cells contain a higher proportion of β-catenin structures with an area > 1 μm^2, which correlated with a decrease in those having an area < 0.2 μm^2 (Fig. 1I). Together, these data indicate an abnormal distribution of β-catenin in animal and cellular models of ALS motor neurons.

3.2. β-catenin structures in NSC34 cells expressing mutant SOD1 do not co-localize with protein aggregates present in ALS and other pathological conditions

Cytoplasmic aggregates of β-catenin have been shown to be phosphorylated in the brains of AD patients (Ghanevati and Miller, 2005). In addition, in cultures of N2a cells treated with proteasome inhibitors, β-catenin aggregates co-localize with vimentin and γ-tubulin, revealing that they form aggresomes (Ghanevati and Miller, 2005). In order to correlate the presence of β-catenin structures with alterations of protein degradation pathways, we conducted a series of double labeling experiments and analyzed them under confocal microscopy (Fig. 2). To analyze if β-catenin accumulation is related to SOD1 aggregation, NSC34 cells were transiently transfected with hSOD1^{WT}-GFP or hSOD1^{G93A}-GFP expression vectors and then treated with the proteasome inhibitor MG132 (Onesto et al., 2011). MG132 treatment enhanced the accumulation of hSOD1^{G93A}-GFP; however, these structures did not co-localize with β-catenin (Fig. 2A), suggesting the presence of distinct and independent protein accumulations. We then monitored the distribution of ubiquitin-positive aggregates after proteasome inhibition. Our results show that incubation of NSC34-hSOD1^{G93A} cells with MG132 resulted in the formation of ubiquitin-positive inclusions but they do not distribute along with β-catenin (Fig. 2B). Similarly, β-catenin structures did not co-localize with γ-tubulin (Fig. 2C), a marker of perinuclear aggresomes (Ghanevati and Miller, 2005; Johnston et al., 1998). These results indicate that β-catenin structures do not distribute with aggregates cleared by the main protein degradation pathways.

We next evaluated other markers of protein aggregation occurring in neurodegenerative diseases. We first analyzed stress granules, since the accumulation of these structures often involves different proteins altered in ALS implicated in RNA metabolism, controlling translational rates upon proteostasis defects (Medinas et al., 2017; Taylor et al., 2016). In order to define if β-catenin structures interact with stress granules, NSC34-hSOD1 cells were treated with sodium arsenite to induce stress granule assembly and then co-immunolabeled with the specific markers TIA1 and eIF3h (Fig. 2D). We found that sodium arsenite treatment triggered the formation of stress granules in cells expressing WT and mutant SOD1 (Fig. 2D). Quantification shows that although the number of stress granules per cell decreases (Fig. 2E), the

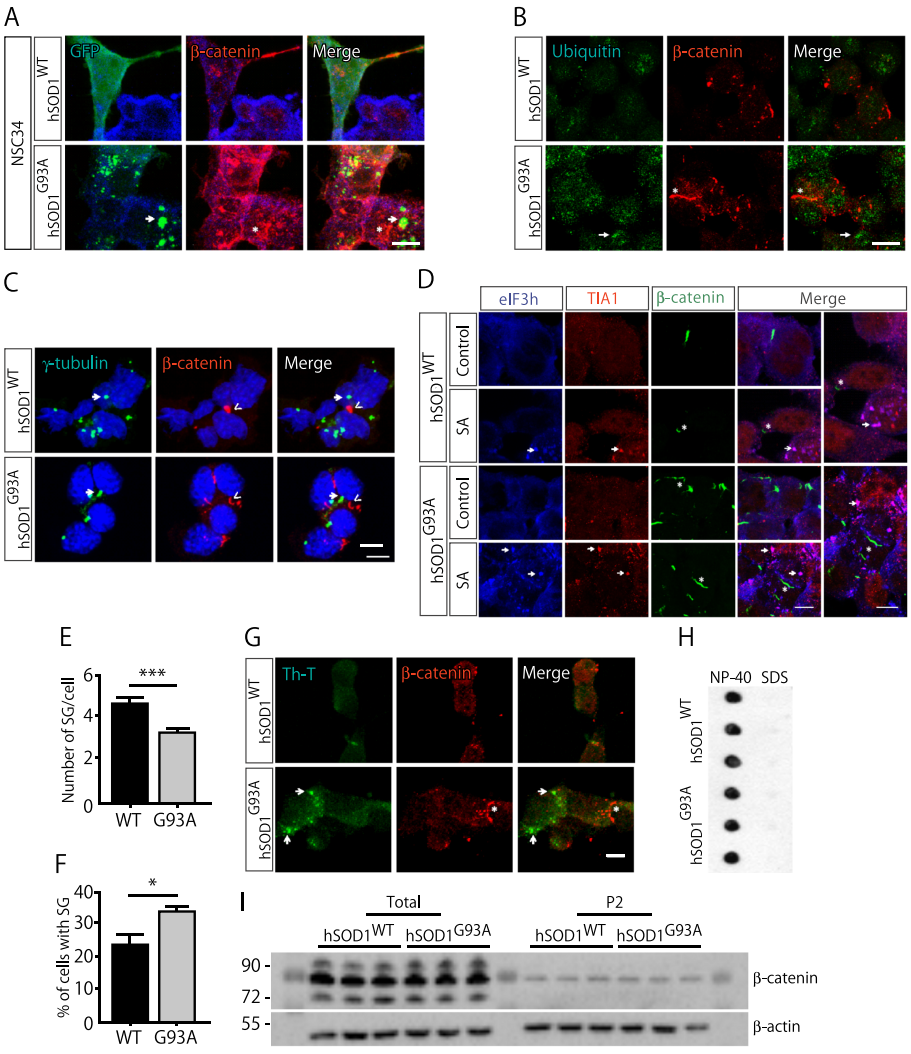

Fig. 2. β-catenin structures do not co-distribute with protein aggregates in NSC34-hSOD1^{G93A} cells.
(A) NSC34 cells were transfected with plasmids coding for hSOD1^{WT} or hSOD1^{G93A} fused to GFP and treated with the proteasome inhibitor MG132 during 6 h. Cells were stained against β-catenin (red) and MAP1B (blue). (B) NSC34-hSOD1 cells were treated with MG132 and co-stained against β-catenin (red) and Ubiquitin (green). Ubiquitin aggregates (arrows) do not co-distribute with β-catenin structures (asterisks). (C) NSC34-hSOD1 cells were co-stained to detect β-catenin (red) and the aggresome marker γ-tubulin (green). β-catenin structures (arrowhead) do not co-localize with γ-tubulin (arrow). (D) NSC34-hSOD1 cells were treated with sodium arsenite (SA), fixed and subsequently subjected to staining with antibodies against eIF3h (blue), TIA1 (red), and β-catenin (green). Nuclei were counterstained with DAPI. Even though arsenite treatment induced stress granule formation in both NSC34-hSOD1 cell lines, evidenced by eIF3h and TIA1 co-localization (arrows), they did not co-distribute with β-catenin structures (asterisks). (E) Quantifications of the number of stress granules per cell and (F) the percentage of cells with stress granules. (G) To reveal amyloid structures, NSC34-hSOD1 cells were incubated with ThT-488 (green) and stained against β-catenin (red). Amyloid aggregates (arrows) do not co-distribute with β-catenin structures (asterisk). Scale Bars = 10 μm. (H) Total protein extracts from three different cultures of NSC34-hSOD1 cells were diluted in PBS containing Nonidet P-40 (NP-40) or SDS and analyzed by filter-trap for detection of β-catenin aggregates. (I) Protein extracts from (H) were also fractionated into NP-40-insoluble pellet (P2) and analyzed by Western-blot for detection of β-catenin. β-actin was employed as loading control. (For interpretation of the references to colour in this figure legend, the reader is referred to the web version of this article.)

percentage of cells containing stress granules is increased in cells expressing mutant SOD1 (Fig. 2F). In addition, our findings show that β-catenin did not co-distribute with stress granules (Fig. 2D). Next, we considered to evaluate the accumulation of protein aggregates with amyloid properties, formed of insoluble β-sheet structures, as they are present in most neurodegenerative diseases, including fALS (Bigio et al., 2013; Soto, 2003). Interestingly, our results show that NSC34-hSOD1^{G93A} cells display increased amyloid aggregates, as evidenced by thioflavin T-488 (ThT) staining. However, ThT-positive aggregates did not co-distribute with β-catenin in these cells (Fig. 2G). We finally performed analyses to assess biochemical properties of β-catenin in NSC34 cells. Using filter-trap assays we detected similar levels of β-catenin species larger than 0.22 μm in protein extracts of both NSC34-hSO1^{G93A} and NSC34-hSOD1^{WT} cells diluted with the non-ionic detergent Nonidet P-40 (Fig. 2H, NP-40). However, the addition of the denaturing ionic detergent SDS solubilized these β-catenin species, preventing the detection by filter-trap (Fig. 2H, SDS). These results indicate that the β-catenin cytosolic accumulations observed in ALS motor neurons do not exhibit features of common protein aggregates, consistently with the lack of localization with ubiquitinated or amyloid structures (Fig. 2B and G). Next, we isolated NP-40-insoluble β-catenin species using centrifugal sedimentation followed by Western-blot analyses. Similar low levels of β-catenin were detected in the insoluble pellet of NSC34-hSO1^{G93A} and NSC34-hSOD1^{WT} protein extracts (Fig. 2I), in line with the filter-trap results. Taken together, our findings show a significant increase in the number and size of β-catenin structures in ALS-like NSC34 cells. Nevertheless, β-catenin accumulations present in NSC34-hSOD1^{G93A} cells were not associated to common protein aggregates cleared by degradative pathways or to those that have been described in ALS and other neurodegenerative diseases, such as stress granules, amyloid aggregates, and SDS-resistant species.

3.3. Impaired cell-cell interaction and increased cell-cell coupling correlate with the presence of β-catenin structures in cells expressing mutant SOD1

In addition to act as an essential effector of Wnt-mediated gene expression, β-catenin plays key roles in cell-cell interactions (Daugherty and Gottardi, 2007). As β-catenin accumulation occurs mainly at the periphery of clustered NSC34-hSOD1^{G93A} cells, we first analyzed the potential co-localization with N- or E-cadherin (Fig. 3A,B). N-cadherin distributes as dots with low frequency in cell-cell interfaces in both NSC34-hSOD1 cell lines (Fig. 3A). Although a small fraction of N-cadherin puncta co-localize with β-catenin in control NSC34-hSOD1^{WT} cells, the large β-catenin structures of NSC34-hSOD1^{G93A} cells did not co-distribute with N-cadherin (Fig. 3A). E-cadherin also displays a punctate distribution in both NSC34-hSOD1 cell lines, although more abundant than those of N-cadherin. Double staining shows that β-catenin partially co-localizes with E-cadherin (Fig. 3B). The Mander's overlap coefficient was determined to quantify the degree of co-distribution between both proteins in cell-cell appositional and non-appositional zones. Our findings show impaired co-localization of β-catenin and E-cadherin in NSC34 cells expressing the G93A mutated form

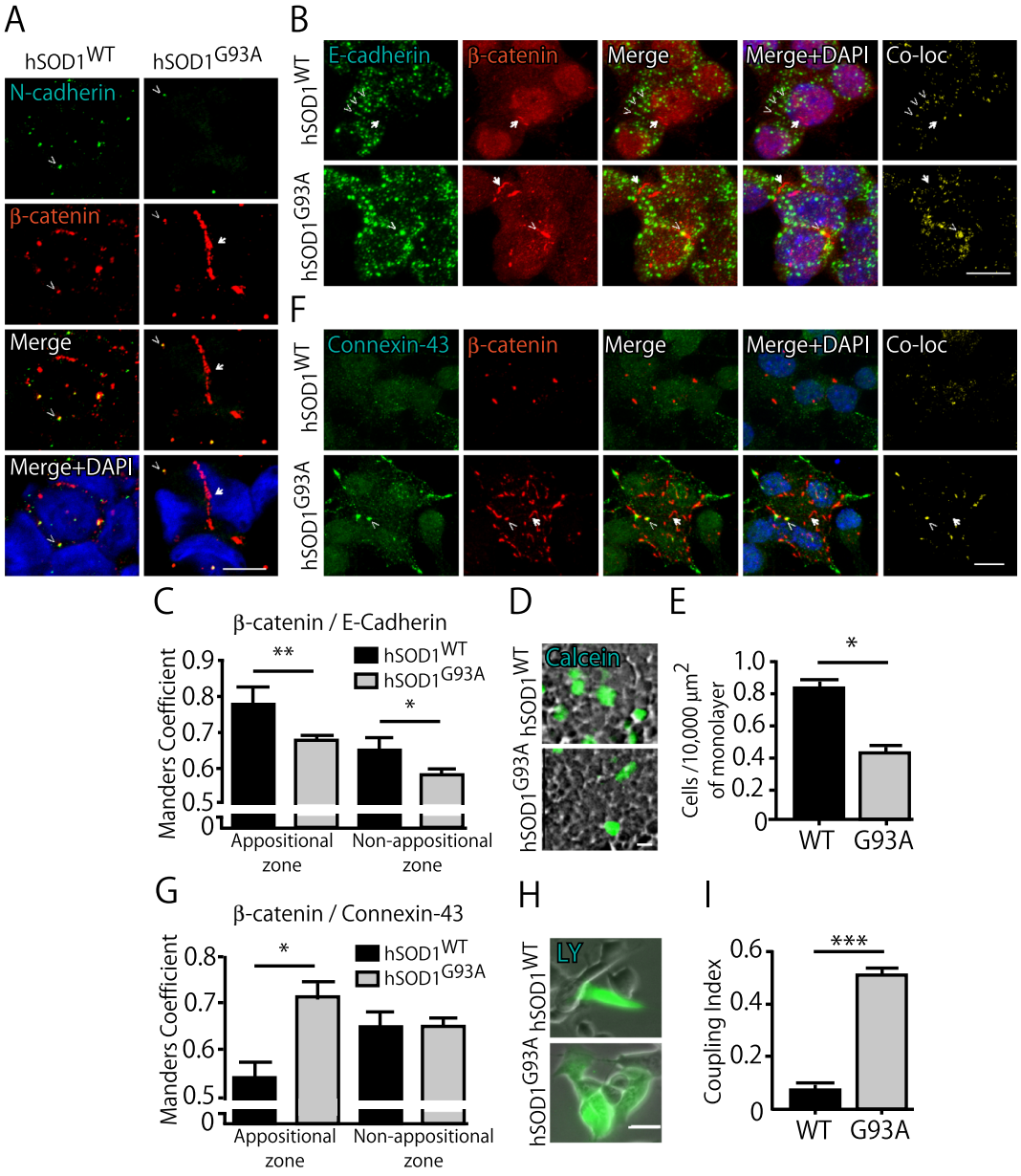

Fig. 3. NSC34-hSOD1^{G93A} cells display impaired cell-cell interaction and increased cell-cell coupling.
NSC34-hSOD1 cells were co-stained to reveal β-catenin (red) along with (A) N-cadherin or (B) E-cadherin (green). Nuclei were counterstained with DAPI (blue). β-catenin structures (arrows) do not co-localize with N-cadherin (A, arrowheads) and partially co-localizes with E-cadherin puncta (B, arrowheads), as evidenced by image processing to reveal the co-localization regions (yellow, *right panel*). (C) Mander's overlap coefficient quantification between β-catenin and E-cadherin in cell-cell appositional and non-appositional zones. (D) NSC34-hSOD1 cells were loaded with the live-cell Calcein AM-488 dye (green), trypsinized, and subjected to bind to monolayers of their corresponding cell line (bright field) for 30 min at 37 °C. (E) Quantification of cell-cell adhesion expressed as the number of cells per 10,000 µm^2 of cell monolayer. Data are the mean ± SEM of three independent experiments (*$p < 0.05$). (F) NSC34-hSOD1 cells were co-stained to detect β-catenin (red) and Connexin-43 (green). Nuclei were counterstained with DAPI (blue). β-catenin structures (arrows) partially co-localize with Connexin-43 (arrowheads). Image processing reveals the co-localization regions (yellow, *right panel*) (G) Mander's overlap analyses between β-catenin and Connexin-43 in cell-cell appositional and non-appositional zones. (H) NSC34-hSOD1 cells were co-injected with Lucifer yellow/Neurobiotin dyes. After 2 min, the dye transference to adjacent cells was analyzed by epifluorescence microscopy. The panels show superimposed phase-contrast and Lucifer yellow fluorescence. (I) Quantification of coupling index, expressed as the mean ± SEM of three independent experiments (***$p < 0.001$, *t*-test). Scale Bars = 10 µm (A,B,D,F,H). (For interpretation of the references to colour in this figure legend, the reader is referred to the web version of this article.)

of SOD1 in both subcellular regions (Fig. 3C). To analyze cell-cell interactions at the functional level, NSC34-hSOD1 cells were labeled with the membrane-permeable live-cell Calcein AM dye, trypsinized, and subjected to bind to monolayers of their corresponding cell line for 30 min (Fig. 3D). Quantification shows that both NSC34-hSOD1 cells bind to a monolayer of their corresponding cell line; however, this ability is significantly impaired in NSC34-hSOD1^{G93A} cells (Fig. 3E).

Secondly, we focused on evidence pointing to β-catenin co-distribution with gap junctions (Ai et al., 2000; Rinaldi et al., 2015). Indeed, in cardiomyocytes, β-catenin interacts with Connexin-43 (Ai et al., 2000), a gap junction-forming protein whose expression increases in the motor cortex and the spinal cord of ALS patients (Almad et al., 2016). Thus, we co-stained NSC34-hSOD1 cells with antibodies against β-catenin and Connexin-43 (Fig. 3F). Quantification of the Mander's overlap coefficient shows that both proteins co-distribute in cell-cell appositional and non-appositional zones in both cell types; remarkably,

the co-distribution of β-catenin and Connexin-43 is significantly increased in the appositional zone of NSC34-hSOD1^{G93A} cells (Fig. 3G). To functionally analyze gap junctions in NSC34-hSOD1 cells, we examined intercellular dye transfer coupling (Martinez et al., 2002). To this aim, Lucifer yellow/neurobiotin were injected into single cells from cell groups of both NSC34-hSOD1 cell lines and after 2 min the presence of both tracers in adjacent cells was analyzed as a measure of cell coupling. In NSC34-hSOD1^{WT} cells, dyes remained restricted to the micro-injected cell; in turn, most of the microinjected NSC34-hSOD1^{G93A} cells showed dye diffusion to two or more adjacent cells (Fig. 3H). Quantification of the coupling index shows a strong and significant increase of the coupling between NSC34-hSOD1^{G93A} cells, compared to control NSC34-hSOD1^{WT} cells (hSOD1^{WT}: 0.07 ± 0.01; hSOD1^{G93A}: 0.5 ± 0.01; ***$p < 0.001$) (Fig. 3I). Together, our findings show that the presence of peripheral β-catenin structures in NSC34 cells expressing mutant hSOD1 correlates with impaired cell-cell adhesion and increased cell-cell coupling.

3.4. GSK3β inhibition induces the disassembly of β-catenin structures in mutant SOD1 expressing cells

The subcellular distribution of β-catenin in the membrane, the cytosol and the nucleus is regulated by its phosphorylation by GSK3β (Wu and Pan, 2010). To gain further insights on β-catenin accumulation in ALS-like motor neurons, NSC34-hSOD1^{G93A} cells were treated with pharmacological agents that inhibit GSK3β. Western blot experiments showed that total β-catenin levels were similar in control and NSC34-hSOD1^{G93A} cells, consistent with our previously published results (Pinto et al., 2013). As expected, we found that both, lithium chloride and Andrographolide (ANDRO) treatments, increased β-catenin levels in control NSC34-hSOD1^{WT} cells, demonstrating that both drugs inhibit GSK3β. Nevertheless, both drugs failed in increasing total β-catenin levels in NSC34-hSOD1^{G93A} cells (Fig. 4A-B). Remarkably, we found that the treatment of undifferentiated NSC34-hSOD1^{G93A} cells with lithium chloride significantly reduced the number of β-catenin structures (PBS: 2.9 ± 0.48; LiCl: 1.2 ± 0.10; *$p < 0.05$) and their average area (Fig. 4C-E). Histogram analyses revealed that lithium treatment resulted in a lower proportion of β-catenin structures with an area > 1 μm^2 which correlated with an increase in those having an area < 0.2 μm^2 (Fig. 4F). Comparable results were obtained with the more specific GSK3β inhibitor ANDRO (Tapia-Rojas et al., 2015) (Fig. 4G). ANDRO treatment reduced the number of β-catenin structures in NSC34-hSOD1^{G93A} cells (DMSO: 2.5 ± 0.2; ANDRO: 1.1 ± 0.1; *$p < 0.05$) and decreased the average area of these structures (DMSO: 0.7 ± 0.1 μm^2; ANDRO: 0.3 ± 0.04 μm^2; *$p < 0.05$) (Fig. 4G-I). Analyses of size distribution show that ANDRO treatment induced a marked decrease in the proportion of β-catenin structures with an area > 1 μm^2 and a corresponding significant increase in those with an area < 0.2 μm^2 (Fig. 4J). These results indicate that GSK3β inhibition induces the disassembly of β-catenin structures in cells expressing mutant hSOD1.

3.5. Decreased neurite outgrowth triggered by mutant SOD1 is counteracted by GSK3β inhibition

As one of the main features of cellular models of ALS motor neurons is their impaired ability to differentiate into a neuronal-like phenotype (Chen et al., 2014; Gomes et al., 2008; Isobe et al., 2015; Lee et al., 2002; Magrane et al., 2009; Pinto et al., 2013; Yao et al., 2013), we next evaluated the potential effect of GSK3β inhibition on neuronal differentiation. To this aim, NSC34-hSOD1 cells were incubated with lithium chloride during 24 h, differentiated, and subsequently stained against MAP1B for morphological quantification (Benavente et al., 2012; Pinto et al., 2013). In control conditions, the number of differentiated cells was significantly impaired in NSC34-hSOD^{G93A} cells (Fig. 5A), as we reported before (Pinto et al., 2013). Interestingly, lithium treatment rescued the ability of NSC34-hSOD^{G93A} cells to project neurites (Fig. 5A). Quantification indicated that lithium treatment results in a significant increase in the proportion of NSC34-hSOD^{G93A} cells projecting neurites after induction of neuronal differentiation (PBS: 13.0 ± 0.4%; lithium: 24.2 ± 2.5%; *$p < 0.05$, ANOVA) (Fig. 5B). However, the average length of these projections was unaltered by lithium treatment (Fig. 5C). A similar response was exerted by the specific GSK3β inhibitor ANDRO (Fig. 5D). Indeed, ANDRO treatment significantly increased the number of NSC34-hSOD^{G93A} cells having neurites after induction of differentiation (DMSO: 22.0 ± 2.4%; ANDRO: 55.9 ± 2.3%; ***$p < 0.001$). Remarkably, even in undifferentiated cultures treatment with ANDRO resulted in a marked increase in the proportion of cells projecting neurites in NSC34-hSOD1^{G93A} cells (DMSO: 5.1 ± 2.1%; ANDRO: 18.9 ± 3.1%; *$p < 0.05$) (Fig. 5E). Similar to lithium treatment, GSK3β inhibition with ANDRO did not affect the average length of neurites (Fig. 5F). Together, our findings show that GSK3β inhibition disassembles β-catenin structures and rescues the morphological differentiation of an *in vitro* model of ALS motor neurons.

4. Discussion

ALS models bearing the G93A mutation of SOD1 were chosen for this study as their pathological and clinical features are similar to those of ALS patients (Gurney et al., 1994). We have focused on Wnt signaling as several developmental morphogens, including Wnt ligands, regulate numerous aspects of neuronal behavior (Ciani and Salinas, 2005; Inestrosa and Arenas, 2010). Moreover, proteins associated to Wnt-dependent signaling pathways are expressed in the adult brain and have been involved in neuroprotection (Inestrosa and Arenas, 2010; Purro et al., 2014). In the context of ALS, symptomatic stages of the disease display increased levels of transcripts coding for Wnt ligands, receptors, and inhibitors (Al-Chalabi and Hardiman, 2013; González-Fernández et al., 2019; Li et al., 2013). On the other hand, NSC34-hSOD1^{G93A} cells show decreased basal levels of Wnt-dependent transcription (Pinto et al., 2013). Together, this evidence suggests that Wnt pathway inhibition could be associated to ALS. We have previously shown that β-catenin, a key effector of Wnt pathway activation, distribute in supramolecular structures in NSC34 cells bearing the G93A mutation of SOD1 (Pinto et al., 2013). As β-catenin accumulation correlates with decreased Wnt signaling in this *in vitro* ALS model, here we have aimed to characterize β-catenin structures as well as their potential functional outcome in the context of ALS.

Protein aggregates are a common feature of neurodegenerative diseases (Medinas et al., 2018; Takalo et al., 2013) and imply alterations in the protein degradation systems, such as UPS and autophagy activation (Bendotti et al., 2012). Indeed, ALS models show alterations in the protein degradation pathways. For instance, decreased activity of the UPS leads to ubiquitin accumulation (Bendotti et al., 2012) and to aggresome formation (Johnston et al., 2000). In models of different neurodegenerative diseases, such as AD and HD, β-catenin distributes in aberrant patterns, including ubiquitinated β-catenin aggregates and aggresomes (Ghanevati and Miller, 2005; Godin et al., 2010). Based on these findings, we aimed to correlate the distribution of β-catenin structures with the distribution of markers of protein aggregation. We found that β-catenin is not associated with SOD1^{G93A} aggregates, or with a specific pathway of protein degradation, nor forming stress granules. We also analyzed amyloid aggregates, a common feature of neurodegeneration. Indeed, the central structure of protein aggregates involved in AD (Aβ peptide), PD (α-synuclein), and HD (poly-glutaminated proteins) form amyloid structures (Soto, 2003). Amyloid aggregates have also been described in models of mutant proteins causing fALS, as mutations in TDP-43 and FUS (Bendotti et al., 2012). However, the presence of these aggregates in models of SOD1-mediated ALS is less clear (Furukawa et al., 2008; Kerman et al., 2010). Even though our present findings support the notion that amyloid structures are present

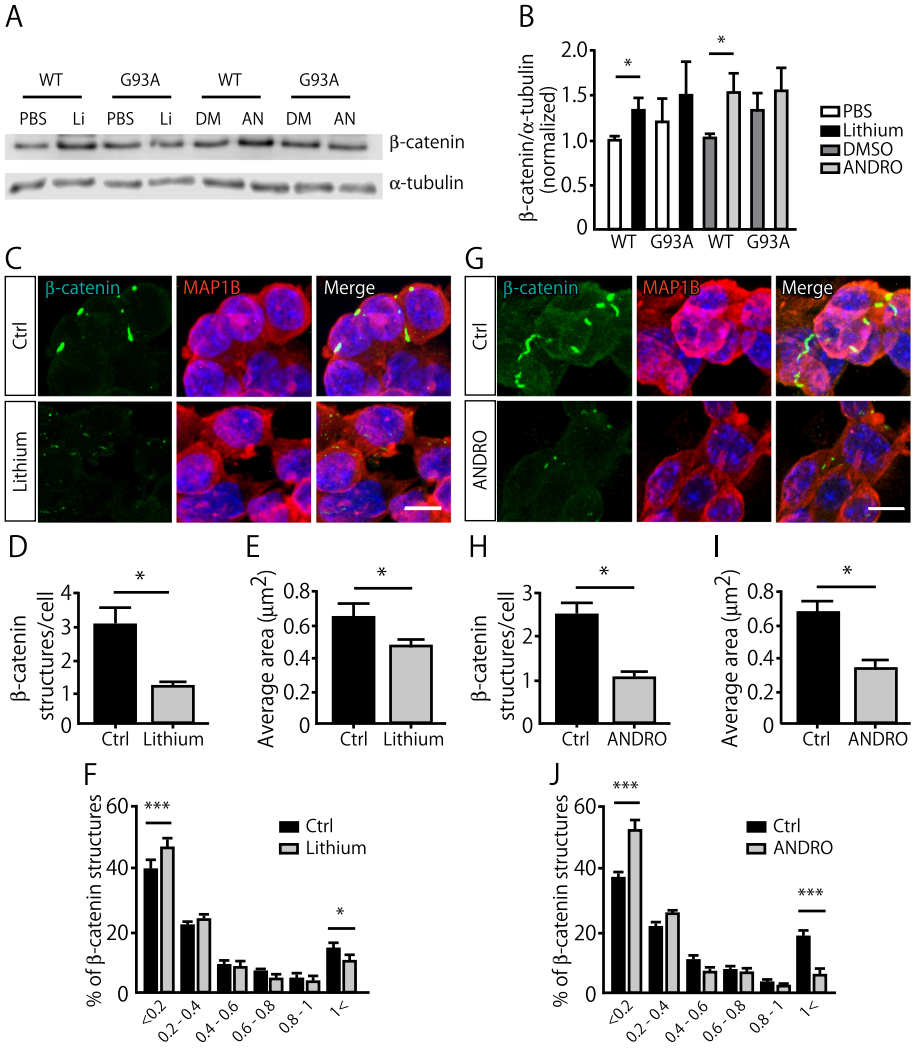

Fig. 4. GSK3β inhibition disassembles β-catenin structures in NSC34-hSOD1^{G93A} cells.
(A) Total protein extracts from NSC34-hSOD1^{G93A} and control NSC34-hSOD1^{WT} cells were analyzed by Western blot using a specific antibody to detect β-catenin. The levels of α-tubulin were used as loading control. (B) Quantification of the relative levels of β-catenin was performed by band intensity densitometry and expressed as a ratio regarding α-tubulin band intensity. Data are expressed as the mean ± SEM of three independent experiments (*$p < 0.05$). NSC34-hSOD1 cells were treated with 40 mM lithium chloride (C-F) or 10 μM ANDRO (G-J) for 6 h. Fixed cells were subsequently subjected to immunocytochemical staining to reveal β-catenin (green) and MAP1B (red). Nuclei were counterstained with DAPI (blue). Quantifications show (D,H) the number of β-catenin aggregate-like structures per cell, (E,I) their average area, and (F,J) their size distribution. Data are the mean ± SEM of three independent experiments (*$p < 0.05$, ***$p < 0.001$, *t*-test). Scale Bars = 10 μm (C,G). (For interpretation of the references to colour in this figure legend, the reader is referred to the web version of this article.)

in ALS models, β-catenin did not co-distribute with these protein aggregates.

What is the nature of the β-catenin structures present in NSC34 cells expressing hSOD^{G93A}? Our filter-trap and aggregate isolation assays reinforce the idea that β-catenin do not form classical insoluble protein aggregates. In this regard, β-catenin aggregates described in brain neurons from AD patients correspond to granulovacuolar degeneration bodies; however, these inclusions have 3 to 5 μm of diameter and are characterized by the presence of ubiquitin (Ghanevati and Miller, 2005; Murata-Shinozaki et al., 2017), different to what we found in β-catenin structures of NSC34-hSOD1^{G93A} cells. One intriguing possibility is that β-catenin assembles as amorphous aggregates, characterized by a three-dimensional structure in which monomers are randomly assembled (Stranks et al., 2009), that have been associated to neurodegeneration. For instance, the microtubule-associated protein tau forms amorphous aggregates in neurofibrillary tangles found in AD patients and in models of frontotemporal dementia (Qureshi et al., 2013; Vogelsberg-Ragaglia et al., 2000). Also, a subset of the α-synuclein protein assemble as amorphous aggregates in models of PD (Uversky and Eliezer, 2009). Interestingly, in the presence of lipid vesicles, hSOD1 assembles amorphous cytotoxic aggregates *in vitro* (Choi et al., 2011). The possibility that β-catenin form amorphous aggregates in the context of ALS motor neurons and their potential involvement in the onset of ALS are attractive avenues for future research.

How does β-catenin become accumulated in ALS-like motor neurons? The dual role of β-catenin in Wnt-mediated gene expression and cell-cell interactions has been related to different pools of the protein (Daugherty and Gottardi, 2007; McCrea et al., 2015). One possible level to regulate the availability of β-catenin pools relies on its interacting proteins at different cell compartments (McCrea et al., 2015). In this regard, our results of the exploration of the β-catenin interactions in the ALS context indicate that even though this protein partially distributes with E-cadherin in control cells, this co-localization is impaired in NSC34-hSOD1^{G93A} cells, which correlates with decreased cell-cell adhesion. It has been well established that cadherin protein levels negatively impact canonical Wnt signaling through binding and sequestering β-catenin from Wnt-dependent transcription (McCrea et al., 2015). Indeed, β-catenin interacts with E-cadherin and Wnt cytosolic effectors in a phosphodestruction complex that, although localized in cell-cell contacts, it is molecularly different from the cadherin–catenin adhesion complex (Maher et al., 2009). A recent elegant study using fly wing imaginal discs show that myosin II-dependent cellular contraction inhibited Wnt target gene transcription by sequestering β-catenin to adherens junctions through its interaction with E-cadherin (Hall et al., 2019). Thus, our results showing decreased β-catenin interaction with E-cadherin in cells expressing mutated hSOD1 could imply an increase in Wnt signaling activation. However, we determined that decreased β-catenin interaction with E-cadherin occurs concomitantly to an increased association with the gap-junction forming protein Connexin-43 that correlated with augmented cell-cell communication. Increased expression of Connexin-43 has been described in both the motor cortex and the spinal cord of ALS patients (Almad et al., 2016). In addition, β-

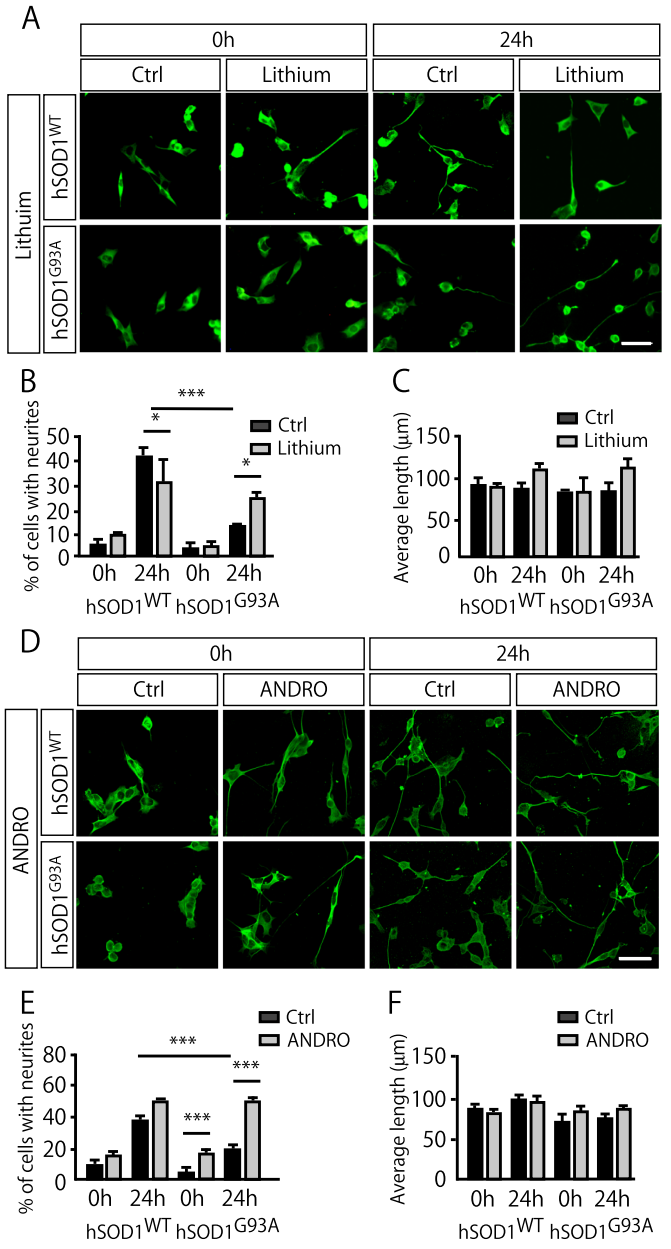

Fig. 5. GSK3β inhibition rescues morphological differentiation of NSC34-hSOD1^{G93A} cells towards a neuron-like phenotype.
NSC34-hSOD1 cells were treated with 100 µM lithium chloride (A-C) or 2 µM ANDRO (D-F) for 24 h and induced to differentiate for additional 24 h. Undifferentiated (0 h) and differentiated (24 h) cells were stained using a specific antibody against MAP1B (green). Morphological parameters of differentiation were quantified as (B,E) the percentage of cells bearing neurites and (C,F) the average length of neurites. Data are the mean ± SEM of three independent experiments (*$p < 0.05$, ***$p < 0.001$). Scale Bars = 50 µm (A,D). (For interpretation of the references to colour in this figure legend, the reader is referred to the web version of this article.)

catenin co-distributes with Connexin-43 in neurospheres of neural progenitor cells obtained from human foetal brain, in mouse cardiac myocytes and in different cell lines (Ai et al., 2000; Hou et al., 2019; Rinaldi et al., 2015). Interestingly, Connexin-43 silencing results in increased Wnt-dependent β-catenin nuclear translocation (Hou et al., 2019) and increases the levels of transcriptionally active β-catenin in neurospheres (Rinaldi et al., 2015). These findings configure a potential scheme where the association of β-catenin with Connexin-43 in cells expressing hSOD1^{G93A} could contribute to the decrease in the transcriptional activity observed in these cells (Pinto et al., 2013).

Another level by which β-catenin pools are regulated relies on its phosphorylation state (McCrea et al., 2015). β-catenin is phosphorylated in sequential steps, where the Casein kinase 1-dependent phosphorylation of Ser45 acts as a priming signal for subsequent GSK3β-dependent phosphorylation of residues Ser33, Ser37 and Thr41 for ubiquitination and proteasome degradation (Daugherty and Gottardi, 2007). Even though β-catenin aggregates present in the context of AD and HD are phosphorylated for degradation (Ghanevati and Miller, 2005; Godin et al., 2010), we found that β-catenin structures in cells expressing hSOD^{G93A} do not co-localize with ubiquitin. How does GSK3β inhibition result in the disassembly of β-catenin structures? GSK3 has been reported to phosphorylate > 40 protein substrates and cumulative evidence reveals that GSK3β regulation can modulate other downstream signaling events independently of β-catenin, including mTOR, BMP, Akt and NFkB1-dependent pathways (Wu and Pan, 2010). Some GSK3β targets are relevant in neurodegenerative conditions, such as tau hyperphosphorylation in a spectrum of tau pathologies, including AD (Iqbal et al., 2010). In the context of ALS, GSK3 is up-regulated in the brain and spinal cord of patients (Yang et al., 2008), where it has been shown to regulate post translational modifications of TDP-43 (Moujalled et al., 2013) and autophagy (de Munck et al., 2016). Accordingly, the use of GSK3 inhibitors exerts positive effects both on stem-cell-derived motor neurons (Yang et al., 2013) and hSOD1^{G93A} transgenic mice, showing improved motor performance (Ahn et al., 2014). Our present findings in motor neuron-like cells expressing hSOD^{G93A} position β-catenin supramolecular complexes as an attractive target to analyze in GSK3β inhibition strategies in the context of ALS.

ALS-like motor neurons display an impaired ability to differentiate into a neuronal-like phenotype. For instance, the expression of hSOD1^{G93A} in NSC34 cells decreases the percentage of cells that develop neuronal processes (Gomes et al., 2008; Lee et al., 2002; Pinto et al., 2013) while motor neurons derived from induced pluripotent stem cells or from human embryonic stem cells display shorter neurites than control cells (Chen et al., 2014; Isobe et al., 2015; Yao et al., 2013). Activation of Wnt signaling by ligand- and drug-dependent inhibition of GSK3β rescues the differentiation of an *in vitro* model of PD neurons (Qi et al., 2017) and plays neuroprotective roles in *in vitro* models of AD (Ardiles et al., 2012; De Ferrari et al., 2003; Purro et al., 2012). How does GSK3β inhibition and the disassembly of β-catenin structures could rescue the morphological differentiation of NSC34-hSOD1^{G93A} cells towards a neuronal-like phenotype? Based on the aforementioned evidence, one possibility is that this effect could be related to transcription. For instance, the increase in β-catenin dependent transcription caused by Connexin-43 silencing in neurospheres results in increased neuronal differentiation (Rinaldi et al., 2015). In addition, incubation of chicken neural tube explants with the CRD domain of Fzd8, which acts antagonizing Wnt signaling, blocks motor neuron differentiation (Nordström et al., 2006). On the other hand, β-catenin could regulate the ability of NSC34-hSOD1^{G93A} cells to extend neurites through local, transcription-independent mechanisms. During the process of neuronal nucleation at the developing spinal cord, cadherin-mediated cell adhesion is crucial for the organization of motor columns; indeed, interfering with β-catenin and α-catenin expression in motor neuron precursors results in an aberrant segregation of the motor columns in the spinal cord (Demireva et al., 2011; Price et al., 2002), likely inducing defects in the organization of sensorial-motor circuits (Sürmeli et al., 2011). Therefore, possible alterations in cell-cell adhesion during early nervous system development that, in our ALS cellular model correlate with altered β-catenin distribution, will potentially result in delayed neuronal differentiation or impaired organization of motor columns. Also, it has been shown that the expression of a stabilized form of β-catenin significantly decreased the proportion of PC12 cells projecting neurites in response to NGF, also through a transcription-independent pathway (Votin et al., 2005). Rather, the mechanism involves adenomatous polyposis coli (APC), a protein belonging to the

β-catenin destruction complex that becomes disassembled upon Wnt pathway activation (Ciani and Salinas, 2005). In these studies, stabilized β-catenin binding to APC blocks the cytoskeleton-dependent ability of APC to induce neurite outgrowth (Votin et al., 2005). Therefore, addressing transcriptional or local signaling responses elicited by GSK3β inhibition will be essential to define its impact on the disassembly of the macromolecular structures formed by β-catenin as well as on neuronal differentiation. These studies will also allow to test for possible pharmacological strategies to manipulate β-catenin accumulation and its potential impact in ALS progression.

Acknowledgements

We thank Drs. Brigitte van Zundert, Lisette Leyton, Federico Bátiz, Luis Aguayo, Teresa Caprile, Christian Peters, and Viviana Pérez for their contribution to these studies. We also thank Pablo Rozas for technical assistance. This work was funded by research grants from Fondo Nacional de Desarrollo Científico y Tecnológico Chile (FONDECYT) 1130321, 1170614 (to JPH), 1140549 (to CH), 1160731 (to AFC), 1171240 (to ADM) and 11150579 (to DM). Additionally, this work was funded by Fondo de Financiamiento de Centros de Investigación en Áreas Prioritarias Chile (FONDAP) program 15150012, the Millennium Institute Chile P09-015-F, Fondo de Fomento al Desarrollo Científico y Tecnológico Chile (FONDEF) ID16I10223 and D11E1007, CONICYT-Brazil 441921/2016-7, the ALS Therapy Alliance 2014-F-059, the Muscular Dystrophy Association 382453, and the ALSRP Therapeutic Idea Award 81XWH-16-1-0112, the US Office of Naval Research-Global (ONR-G) N62909-16-1-2003, the US Air Force Office of Scientific Research FA9550-16-1-0384, the Michael J. Fox Foundation for Parkinson's Research – Target Validation grant no. 9277 (to CH), Muscular Dystrophy Association 575897, ALS Association 468 (to DM) and The Centro Interdisciplinario de Neurociencia de Valparaiso Millennium Institute (P09-022-F) (to ADM).

References

Ahn, S.-W., Jeon, G.S., Kim, M.-J., Shon, J.-H., Kim, J.-E., Shin, J.-Y., Kim, S.-M., Kim, S.H., Ye, I.-H., Lee, K.-W., 2014. Neuroprotective effects of JGK-263 in transgenic SOD1-G93A mice of amyotrophic lateral sclerosis. J. Neurol. Sci. 340, 112–116.

Ai, Z., Fischer, A., Spray, D.C., Brown, A.M., Fishman, G.I., 2000. Wnt-1 regulation of connexin43 in cardiac myocytes. J. Clin. Invest. 105, 161–171.

Al-Chalabi, A., Hardiman, O., 2013. The epidemiology of ALS: a conspiracy of genes, environment and time. Nat. Rev. Neurol. 9, 617.

Almad, A.A., Doreswamy, A., Gross, S.K., Richard, J.P., Huo, Y., Haughey, N., Maragakis, N.J., 2016. Connexin 43 in astrocytes contributes to motor neuron toxicity in amyotrophic lateral sclerosis. Glia. 64, 1154–1169.

Amendola, J., Verrier, B., Roubertoux, P., Durand, J., 2004. Altered sensorimotor development in a transgenic mouse model of amyotrophic lateral sclerosis. Eur. J. Neurosci. 20, 2822–2826.

Ardiles, Á.O., Tapia-Rojas, C.C., Mandal, M., Alexandre, F., Kirkwood, A., Inestrosa, N.C., Palacios, A.G., 2012. Postsynaptic dysfunction is associated with spatial and object recognition memory loss in a natural model of Alzheimer's disease. Proc. Natl. Acad. Sci. 109, 13835–13840.

Benavente, F., Pinto, C., Parada, M., Henríquez, J.P., Osses, N., 2012. Bone morphogenetic protein 2 inhibits neurite outgrowth of motor neuron-like NSC-34 cells and upregulates its type II receptor. J. Neurochem. 122, 594–604.

Bendotti, C., Marino, M., Cheroni, C., Fontana, E., Crippa, V., Poletti, A., De Biasi, S., 2012. Dysfunction of constitutive and inducible ubiquitin-proteasome system in amyotrophic lateral sclerosis: implication for protein aggregation and immune response. Prog. Neurobiol. 97, 101–126.

Bigio, E.H., Wu, J.Y., Deng, H.-X., Bit-Ivan, E.N., Mao, Q., Ganti, R., Peterson, M., Siddique, N., Geula, C., Siddique, T., 2013. Inclusions in frontotemporal lobar degeneration with TDP-43 proteinopathy (FTLD-TDP) and amyotrophic lateral sclerosis (ALS), but not FTLD with FUS proteinopathy (FTLD-FUS), have properties of amyloid. Acta Neuropathol. 125, 463–465.

Bosco, D.A., Lemay, N., Ko, H.K., Zhou, H., Burke, C., Kwiatkowski, T.J., Sapp, P., McKenna-Yasek, D., Brown, R.H., Hayward, L.J., 2010. Mutant FUS proteins that cause amyotrophic lateral sclerosis incorporate into stress granules. Hum. Mol. Genet. 19, 4160–4175.

Cashman, N.R., Durham, H.D., Blusztajn, J.K., Oda, K., Tabira, T., Shaw, I.T., Dahrouge, S., Antel, J.P., 1992. Neuroblastoma x spinal cord (NSC) hybrid cell lines resemble developing motor neurons. Dev. Dyn. 194, 209–221.

Chen, H., Qian, K., Du, Z., Cao, J., Petersen, A., Liu, H., Blackbourn IV, L.W., Huang, C.-L., Errigo, A., Yin, Y., 2014. Modeling ALS with iPSCs reveals that mutant SOD1 misregulates neurofilament balance in motor neurons. Cell Stem Cell 14, 796–809.

Choi, I., Huh, Y.S., Erickson, D., 2011. Size-selective concentration and label-free characterization of protein aggregates using a Raman active nanofluidic device. Lab Chip 11, 632–638.

Ciani, L., Salinas, P.C., 2005. Signalling in neural development: WNTS in the vertebrate nervous system: from patterning to neuronal connectivity. Nat. Rev. Neurosci. 6, 351–362.

Ciechanover, A., Kwon, Y.T., 2015. Degradation of misfolded proteins in neurodegenerative diseases: therapeutic targets and strategies. Exp. Amp. Mol. Med. 47, e147.

Daugherty, R.L., Gottardi, C.J., 2007. Phospho-regulation of β-catenin adhesion and signaling functions. Physiology 22, 303–309.

De Ferrari, G.V., Chacón, M.A., Barría, M.I., Garrido, J.L., Godoy, J.A., Olivares, G., Reyes, A.E., Alvarez, A., Bronfman, M., Inestrosa, N.C., 2003. Activation of Wnt signaling rescues neurodegeneration and behavioral impairments induced by β-amyloid fibrils. Mol. Psychiatry 8, 195–208.

de Munck, E., Palomo, V., Muñoz-Sáez, E., Perez, D.I., Gómez-Miguel, B., Solas, M.T., Gil, C., Martínez, A., Arahuetes, R.M., 2016. Small GSK-3 inhibitor shows efficacy in a motor neuron disease murine model modulating autophagy. PLoS ONE 11, e0162723.

Demireva, E.Y., Shapiro, L.S., Jessell, T.M., Zampieri, N., 2011. Motor pool position and target topography regulated by β-and γ-catenin activities. Cell 147, 641.

Dobrowolny, G., Martini, M., Scicchitano, B.M., Romanello, V., Boncompagni, S., Nicoletti, C., Pietrangelo, L., De Panfilis, S., Catizone, A., Bouchè, M., Sandri, M., Rudolf, R., Protasi, F., Musarò, A., 2017. Muscle expression of SOD1G93A triggers the dismantlement of neuromuscular junction via PKC-theta. Antioxid. Redox Signal. 28, 1105–1119.

Forsberg, K., Jonsson, P.A., Andersen, P.M., Bergemalm, D., Graffmo, K.S., Hultdin, M., Jacobsson, J., Rosquist, R., Marklund, S.L., Brannstrom, T., 2010. Novel antibodies reveal inclusions containing non-native SOD1 in sporadic ALS patients. PLoS ONE 5, e11552.

Furukawa, Y., Kaneko, K., Yamanaka, K., O'Halloran, T.V., Nukina, N., 2008. Complete loss of post-translational modifications triggers Fibrillar aggregation of SOD1 in the familial form of amyotrophic lateral sclerosis. J. Biol. Chem. 283, 24167–24176.

Ghanevati, M., Miller, C.A., 2005. Phospho-β-catenin accumulation in Alzheimer's disease and in aggresomes attributable to proteasome dysfunction. J. Mol. Neurosci. 25, 79–94.

Godin, J.D., Poizat, G., Hickey, M.A., Maschat, F., Humbert, S., 2010. Mutant huntingtin-impaired degradation of β-catenin causes neurotoxicity in Huntington's disease. EMBO J. 29, 2433–2445.

Gomes, C., Palma, A.S., Almeida, R., Regalla, M., McCluskey, L.F., Trojanowski, J.Q., Costa, J., 2008. Establishment of a cell model of ALS disease: Golgi apparatus disruption occurs independently from apoptosis. Biotechnol. Lett. 30, 603–610.

González-Fernández, C., Gonzalez, P., Andres-Benito, P., Ferrer, I., Rodríguez, F.J., 2019. Wnt signaling alterations in the human spinal cord of amyotrophic lateral sclerosis cases: spotlight on Fz2 and Wnt5a. Mol. Neurobiol. 1–15.

Gurney, M.E., Pu, H., Chiu, A.Y., Dal Canto, M.C., Polchow, C.Y., Alexander, D.D., Caliendo, J., Hentati, A., Kwon, Y.W., Deng, H.X., et al., 1994. Motor neuron degeneration in mice that express a human cu,Zn superoxide dismutase mutation. Science 264, 1772–1775.

Hall, E.T., Hoesing, E., Sinkovics, E., Verheyen, E.M., 2019. Actomyosin contractility modulates Wnt signaling through adherens junction stability. Mol. Biol. Cell 30, 411–426.

Hetz, C., Saxena, S., 2017. ER stress and the unfolded protein response in neurodegeneration. Nat. Rev. Neurol. 13, 477.

Hou, X., Khan, M.R.A., Turmaine, M., Thrasivoulou, C., Becker, D.L., Ahmed, A., 2019. Wnt signaling regulates cytosolic translocation of connexin 43. Am. J. Phys. Regul. Integr. Comp. Phys. https://doi.org/10.1152/ajpregu.00268.2018.

Houser, C.R., Crawford, G.D., Barber, R.P., Salvaterra, P.M., Vaughn, J.E., 1983. Organization and morphological characteristics of cholonergic neurons: an immunocytochemical study with a monoclonal antibody to choline acetyltransferase. Brain Res. 266, 97–119.

Inestrosa, N.C., Arenas, E., 2010. Emerging roles of wnts in the adult nervous system. Nat. Rev. Neurosci. 11, 77–86.

Iqbal, K., Liu, F., Gong, C.-X., Grundke-Iqbal, I., 2010. Tau in Alzheimer disease and related tauopathies. Curr. Alzheimer Res. 7, 656–664.

Isobe, T., Tooi, N., Nakatsuji, N., Aiba, K., 2015. Amyotrophic lateral sclerosis models derived from human embryonic stem cells with different superoxide dismutase 1 mutations exhibit differential drug responses. Stem Cell Res. 15, 459–468.

Johnston, J.A., Ward, C.L., Kopito, R.R., 1998. Aggresomes: a cellular response to misfolded proteins. J. Cell Biol. 143, 1883–1898.

Johnston, J.A., Dalton, M.J., Gurney, M.E., Kopito, R.R., 2000. Formation of high molecular weight complexes of mutant cu,Zn-superoxide dismutase in a mouse model for familial amyotrophic lateral sclerosis. Proc. Natl. Acad. Sci. 97, 12571–12576.

Kerman, A., Liu, H.-N., Croul, S., Bilbao, J., Rogaeva, E., Zinman, L., Robertson, J., Chakrabartty, A., 2010. Amyotrophic Lateral Sclerosis is a Non-Amyloid Disease in which Extensive Misfolding of Sod1 is Unique to the Familial form.

Kiernan, M.C., Vucic, S., Cheah, B.C., Turner, M.R., Eisen, A., Hardiman, O., Burrell, J.R., Zoing, M.C., 2011. Amyotrophic lateral sclerosis. Lancet 377, 942–955.

Kuo, J.J., Schonewille, M., Siddique, T., Schults, A.N., Fu, R., Bar, P.R., Anelli, R., Heckman, C.J., Kroese, A.B., 2004. Hyperexcitability of cultured spinal motoneurons from presymptomatic ALS mice. J. Neurophysiol. 91, 571–575.

Lee, K.W., Kim, H.J., Sung, J.J., Park, K.S., Kim, M., 2002. Defective neurite outgrowth in aphidicolin/cAMP-induced motor neurons expressing mutant cu/Zn superoxide dismutase. Int. J. Dev. Neurosci. 20, 521–526.

Li, X., Guan, Y., Chen, Y., Zhang, C., Shi, C., Zhou, F., Yu, L., Juan, J., Wang, X., 2013. Expression of Wnt5a and its receptor Fzd2 is changed in the spinal cord of adult amyotrophic lateral sclerosis transgenic mice. Int. J. Clin. Exp. Pathol. 6, 1245.

Magrane, J., Hervias, I., Henning, M.S., Damiano, M., Kawamata, H., Manfredi, G., 2009. Mutant SOD1 in neuronal mitochondria causes toxicity and mitochondrial dynamics abnormalities. Hum. Mol. Genet. 18, 4552–4564.
Maher, M.T., Flozak, A.S., Stocker, A.M., Chenn, A., Gottardi, C.J., 2009. Activity of the β-catenin phosphodestruction complex at cell–cell contacts is enhanced by cadherin-based adhesion. J. Cell Biol. 186, 219–228.
Martinez, A.D., Hayrapetyan, V., Moreno, A.P., Beyer, E.C., 2002. Connexin43 and connexin45 form heteromeric gap junction channels in which individual components determine permeability and regulation. Circ. Res. 90, 1100–1107.
McCrea, P.D., Maher, M.T., Gottardi, C.J., 2015. Nuclear signaling from cadherin adhesion complexes. Curr. Top. Dev. Biol. 129–196 Elsevier.
Medinas, D.B., Valenzuela, V., Hetz, C., 2017. Proteostasis disturbance in amyotrophic lateral sclerosis. Hum. Mol. Genet. 26, R91–R104.
Medinas, D.B., Rozas, P., Martínez Traub, F., Woehlbier, U., Brown, R.H., Bosco, D.A., Hetz, C., 2018. Endoplasmic reticulum stress leads to accumulation of wild-type SOD1 aggregates associated with sporadic amyotrophic lateral sclerosis. Proc. Natl. Acad. Sci. 115, 8209.
Moloney, E.B., de Winter, F., Verhaagen, J., 2014. ALS as a distal axonopathy: molecular mechanisms affecting neuromuscular junction stability in the presymptomatic stages of the disease. Front. Neurosci. 8, 252.
Moujalled, D., James, J.L., Parker, S.J., Lidgerwood, G.E., Duncan, C., Meyerowitz, J., Nonaka, T., Hasegawa, M., Kanninen, K.M., Grubman, A., 2013. Kinase inhibitor screening identifies cyclin-dependent kinases and glycogen synthase kinase 3 as potential modulators of TDP-43 cytosolic accumulation during cell stress. PLoS ONE 8, e67433.
Murata-Shinozaki, Y., Takahashi, T., Matsubara, T., Maruyama, H., Izumi, Y., Matsumoto, M., 2017. The origins of rimmed vacuoles and granulovacuolar degeneration bodies are associated with the Wnt signaling pathway. Neurosci. Lett. 638, 55–59.
Nordström, U., Maier, E., Jessell, T.M., Edlund, T., 2006. An early role for WNT signaling in specifying neural patterns of cdx and Hox gene expression and motor neuron subtype identity. PLoS Biol. 4, e252.
Onesto, E., Rusmini, P., Crippa, V., Ferri, N., Zito, A., Galbiati, M., Poletti, A., 2011. Muscle cells and motoneurons differentially remove mutant SOD1 causing familial amyotrophic lateral sclerosis. J. Neurochem. 118, 266–280.
Pambo-Pambo, A., Durand, J., Gueritaud, J.-P., 2009. Early excitability changes in lumbar motoneurons of transgenic SOD1G85R and SOD1G93A-low mice. J. Neurophysiol. 102, 3627–3642.
Pinto, C., Cardenas, P., Osses, N., Henriquez, J.P., 2013. Characterization of Wnt/beta-catenin and BMP/Smad signaling pathways in an in vitro model of amyotrophic lateral sclerosis. Front. Cell. Neurosci. 7, 239.
Price, S.R., Garcia, N.V.D.M., Ranscht, B., Jessell, T.M., 2002. Regulation of motor neuron pool sorting by differential expression of type II cadherins. Cell 109, 205–216.
Purro, S.A., Dickins, E.M., Salinas, P.C., 2012. The secreted Wnt antagonist Dickkopf-1 is required for amyloid beta-mediated synaptic loss. J. Neurosci. 32, 3492–3498.
Purro, S.A., Galli, S., Salinas, P.C., 2014. Dysfunction of Wnt signaling and synaptic disassembly in neurodegenerative diseases. J. Mol. Cell Biol. 6, 75–80.
Qi, L., Tang, Y., He, W., Pan, H., Jiang, W., Wang, L., Deng, W., 2017. Lithium chloride promotes neuronal differentiation of rat neural stem cells and enhances neural regeneration in Parkinson's disease model. Cytotechnology. 69, 277–287.
Qureshi, H.Y., Li, T., MacDonald, R., Cho, C.M., Leclerc, N., Paudel, H.K., 2013. Interaction of 14-3-3ζ with microtubule-associated protein tau within Alzheimer's disease neurofibrillary tangles. Biochemistry. 52, 6445–6455.
Rinaldi, F., Hartfield, E., Crompton, L., Badger, J., Glover, C., Kelly, C., Rosser, A., Uney, J., Caldwell, M., 2015. Cross-regulation of Connexin43 and β-catenin influences differentiation of human neural progenitor cells. Cell Death Dis. 5, e1017.
Soto, C., 2003. Unfolding the role of protein misfolding in neurodegenerative diseases. Nat. Rev. Neurosci. 4, 49.
Stevens, J.C., Chia, R., Hendriks, W.T., Bros-Facer, V., van Minnen, J., Martin, J.E., Jackson, G.S., Greensmith, L., Schiavo, G., Fisher, E.M.C., 2010. Modification of superoxide dismutase 1 (SOD1) properties by a GFP tag – implications for research into amyotrophic lateral sclerosis (ALS). PLoS ONE 5, e9541.
Stranks, S.D., Ecroyd, H., Van Sluyter, S., Waters, E.J., Carver, J.A., Von Smekal, L., 2009. Model for amorphous aggregation processes. Phys. Rev. E 80, 051907.
Sürmeli, G., Akay, T., Ippolito, G.C., Tucker, P.W., Jessell, T.M., 2011. Patterns of spinal sensory-motor connectivity prescribed by a dorsoventral positional template. Cell. 147, 653–665.
Takalo, M., Salminen, A., Soininen, H., Hiltunen, M., Haapasalo, A., 2013. Protein aggregation and degradation mechanisms in neurodegenerative diseases. Am. J. Neurodegener. Dis. 2, 1–14.
Tapia-Rojas, C., Schüller, A., Lindsay, C.B., Ureta, R.C., Mejías-Reyes, C., Hancke, J., Melo, F., Inestrosa, N.C., 2015. Andrographolide activates the canonical Wnt signalling pathway by a mechanism that implicates the non-ATP competitive inhibition of GSK-3β: autoregulation of GSK-3β in vivo. Biochem. J. 466, 415–430.
Taylor, J.P., Brown, R.H., Cleveland, D.W., 2016. Decoding ALS: from genes to mechanism. Nature 539, 197–206.
Tourrière, H., Chebli, K., Zekri, L., Courselaud, B., Blanchard, J.M., Bertrand, E., Tazi, J., 2003. The RasGAP-associated endoribonuclease G3BP assembles stress granules. J. Cell Biol. 160, 823–831.
Turner, M.R., Hardiman, O., Benatar, M., Brooks, B.R., Chio, A., de Carvalho, M., Ince, P.G., Lin, C., Miller, R.G., Mitsumoto, H., Nicholson, G., Ravits, J., Shaw, P.J., Swash, M., Talbot, K., Traynor, B.J., den Berg, L.H.V., Veldink, J.H., Vucic, S., Kiernan, M.C., 2013. Controversies and priorities in amyotrophic lateral sclerosis. Lancet Neurol. 12, 310–322.
Uversky, V.N., Eliezer, D., 2009. Biophysics of Parkinson's disease: structure and aggregation of α-synuclein. Curr. Protein Pept. Sci. 10, 483–499.
Valentine, J.S., Doucette, P.A., Zittin Potter, S., 2005. Copper-zinc superoxide dismutase and amyotrophic lateral sclerosis. Annu. Rev. Biochem. 74, 563–593.
van Zundert, B., Peuscher, M.H., Hynynen, M., Chen, A., Neve, R.L., Brown, R.H., Constantine-Paton, M., Bellingham, M.C., 2008. Neonatal neuronal circuitry shows Hyperexcitable disturbance in a mouse model of the adult-onset neurodegenerative disease amyotrophic lateral sclerosis. J. Neurosci. 28, 10864–10874.
Vogelsberg-Ragaglia, V., Bruce, J., Richter-Landsberg, C., Zhang, B., Hong, M., Trojanowski, J.Q., Lee, V.M.-Y., 2000. Distinct FTDP-17 missense mutations in tau produce tau aggregates and other pathological phenotypes in transfected CHO cells. Mol. Biol. Cell 11, 4093–4104.
Votin, V., Nelson, W.J., Barth, A.I., 2005. Neurite outgrowth involves adenomatous polyposis coli protein and β-catenin. J. Cell Sci. 118, 5699–5708.
Wu, D., Pan, W., 2010. GSK3: a multifaceted kinase in wnt signaling. Trends Biochem. Sci. 35, 161–168.
Yang, W., Leystra-Lantz, C., Strong, M.J., 2008. Upregulation of GSK3β expression in frontal and temporal cortex in ALS with cognitive impairment (ALSci). Brain Res. 1196, 131–139.
Yang, Y.M., Gupta, S.K., Kim, K.J., Powers, B.E., Cerqueira, A., Wainger, B.J., Ngo, H.D., Rosowski, K.A., Schein, P.A., Ackeifi, C.A., 2013. A small molecule screen in stem-cell-derived motor neurons identifies a kinase inhibitor as a candidate therapeutic for ALS. Cell Stem Cell 12, 713–726.
Yao, X.L., Ye, C.H., Liu, Q., Wan, J.B., Zhen, J., Xiang, A.P., Li, W.Q., Wang, Y., Su, H., Lu, X.L., 2013. Motoneuron differentiation of induced pluripotent stem cells from SOD1G93A mice. PLoS ONE 8, e64720.